BIOLOGY OF REPRODUCTION 34, 613–623 (1986)

Mouse Testicular and Sperm Cell Development Characterized from Birth to Adulthood by Dual Parameter Flow Cytometry[1]

FRANK C. JANCA, LORNA K. JOST,
and DONALD P. EVENSON[2]

Department of Chemistry
South Dakota State University
Brookings, South Dakota 57007

ABSTRACT

Dual parameter flow cytometry was used to investigate cellular changes in male germinal tissue during normal postpartum maturation in B6C3F$_1$/J mice. Animals were killed at 2-day intervals from 2 to 42 days postpartum and at 48, 64, 72, 93 and 100 days postpartum. Testicular, cauda epididymis and vas deferens cell suspensions were stained with the metachromatic fluorochrome acridine orange and measured by flow cytometry for red and green fluorescence levels after excitation by blue laser light. Intensities of red and green fluorescence reflect amounts of single- and double-strand nucleic acid sites available for acridine orange staining, respectively, and were used to classify cells on the basis of ploidy level, RNA content, and chromatin structure, as defined by susceptibility to acid denaturation of DNA in situ. Sperm from cauda epididymis and vas deferens were examined by light microscopy to determine frequency of abnormal sperm head morphology.

Fluorescence data derived from acridine orange-stained testicular cells quantified the sequential changes in 1) proportions of haploid, diploid and tetraploid cell types during the first round of spermatogenesis, and 2) proportions of round, elongating, and elongated spermatids during the first round of spermiogenesis. Ratios of the three major testicular populations (haploid, diploid, and tetraploid) reached adult levels by 48 days postpartum.

Sperm cells were first detected in the cauda epididymis and vas deferens on 30 and 36 days postpartum, respectively. Early sperm populations, compared to adult sperm, exhibited up to 89% abnormalities in sperm head morphology that correlated with significant levels of abnormal chromatin structure. Percentage of sperm head abnormalities and chromatin structure in the cauda epididymis and vas deferens approached normal adult levels by 42 and 48 days postpartum, respectively.

INTRODUCTION

Mammalian spermatogenesis consists of a continuum of biochemical pathways and morphological alterations that can be divided into three major phases: 1) spermatogonial proliferation and renewal, 2) meiosis, and 3) spermiogenesis (Bellvé et al., 1977). During each of these phases, specific changes in cell populations and cell associations occur within the seminiferous tubules (Oakberg, 1956a,b; Clermont and Perey, 1957; Kluin et al., 1984). Spermatogonial proliferation and renewal consists of mitotic proliferation of gonocytes that subsequently evolve into a series of mitotically dividing spermatogonial types, culminating with the formation of preleptotene primary spermatocytes. Reductional and equational divisions of these spermatocytes produce haploid spermatids. Spermiogenesis involves a complex series of morphological and biochemical changes that transform haploid round spermatids into elongated spermatids, and finally into testicular spermatozoa. (Oakberg, 1956a; Millette and Bellvé, 1977; Balhorn et al., 1984; Kleene et al., 1984).

Sperm were one of the first living cells to be observed under the light microscope by Van Leeuwenhoek in 1677 (Schierbeek, 1959). Since then, light microscopy has been utilized extensively to study spermatogenesis in a number of species (Ro-

Accepted October 31, 1985.
Received August 19, 1985.
[1] Although the research described in this article has been funded in part by the Health Effects Research Laboratory, U.S. Environmental Protection Agency, through Grant No. CR 810091 to South Dakota State University, it has not been subjected to the Agency peer and policy review and therefore does not necessarily reflect the views of the Agency and no official endorsement should be inferred. Manuscript No. 2093 from the South Dakota State University Experiment Station.
[2] Reprint requests: Donald P. Evenson, Dept. of Chemistry, South Dakota State University, Animal Science Complex, Box 2170, Brookings, SD 57007.

osen-Runge, 1977). Although the light microscope will remain a powerful and widely used tool, the rapidly emerging technology of flow cytometry (FCM) has distinct advantages in cell analysis, e.g., 1) speed (1000's of cells/ second), 2) objective machine measurements rather than subjective human eye evaluations, 3) analysis of large numbers of cells providing high statistical significance, and 4) unbiased cell sampling.

Single parameter FCM measurements have been used to classify testicular cells in growing (Clausen et al., 1977) and adult (Gledhill et al., 1979) animals. Other studies (Evenson and Melamed, 1983; Evenson et al., 1985) have employed dual parameter FCM to characterize cells from adult mammalian testes.

The metachromatic dye, acridine orange (AO), used in this study intercalates into double-strand (DS) nucleic acid and produces green fluorescence (GF) upon illumination with blue laser light (488nm). Interaction with single-strand (SS) DNA or RNA produces red fluorescence (RF) (Darzynkiewicz et al., 1976, 1983). Quantification of RF and GF has been used to identify haploid (1n; round, elongating and elongated spermatids), diploid (2n) and tetraploid (4n) cell types present in cellular suspensions prepared from minced testicular biopsies (Evenson and Melamed, 1983).

Recent studies (Evenson et al., 1985, 1986a,b) have demonstrated the usefulness of FCM for measuring effects of various chemical agents on alterations of testicular cells with regard to cell killing, proliferation and/or differentiation. Flow cytometry has also been used to demonstrate a quantitative relationship between dose of chemical exposure and alterations of sperm chromatin structure, both correlating with sperm head morphology as assayed by light microscopy (Evenson et al., 1985, 1986a,b).

We are interested in determining the effects of mutagenic and/or cytotoxic chemicals that exhibit stage-specificity in germ cells (Cattanach et al., 1968; Ehling et al., 1968, Sega, 1974) or stage-specificity in reproductive maturation (Carter and Laskey, 1982; Carter et al., 1984). Before effects of these types of agents can be evaluated effectively by FCM, studies using FCM techniques to examine developmental changes in the growing mammalian testis are required. We report here on FCM measurements of AO-stained testicular and sperm cells isolated from untreated prepubertal (2–30 days postpartum (dpp)), pubertal (30–64 dpp), and adult (64–100 dpp) male mice (ages defined by Albert and Roussel, 1983). These data provide background for chemical toxicology studies.

MATERIALS AND METHODS

Experimental Animals

Male B6C3F$_1$/J mice between 30 and 100 (± 0.5) dpp were obtained from Jackson Laboratories (Bar Harbor, ME). Prepubertal (2–28 dpp) males of the same strain were produced at our facilities by crossing C57BL/6J females with C3H/HeJ males (Jackson Laboratories). Litter sizes were limited to 10 pups by culling excess female siblings. Pups were weaned at 21 dpp.

All weanling and older mice were maintained on an ad libitum diet of Purina Rodent Chow (Ralston Purina Co., St. Louis, MO) and deionized water. Animals were housed in plastic cages with wire tops, maintained at constant room temperature (21 ± 2°C) and kept on a 0700 to 1900 h lighting schedule.

Sampling Schedule

Young males were killed at 2-day intervals from 2 to 42 dpp. Older males were killed at 48, 64, 72, 93 and 100 dpp. Three randomly chosen animals were killed for each time point and, immediately following cervical dislocation, testes, epididymides and vas deferens were surgically removed. A stereoscopic dissecting microscope was used to facilitate removal of tissue samples from 2–20 dpp animals. Tissue samples were maintained on ice (4°C) in buffer solutions, specified below, throughout the remaining procedures. Testes and cauda epididymis (cauda) were dissociated with curved surgical scissors into cellular suspensions and transferred into 12 × 75 mm conical bottom polystyrene culture tubes (Fisher Scientific Co., Pittsburgh, PA). After allowing several min for tissue fragments to settle out, the supernatant was filtered through appropriate gauge Nitex nylon filters (Tetko Inc., Elmsford, NY).

Testicular Cells

Testes were minced in Hank's Balanced Salt Solution (HBSS: Gibco Laboratories, Grand Island, NY) and the liberated cells filtered through 53 μm nylon filters.

Cauda Epididymal Sperm Cells

Cauda epididymides were minced in TNE buffer [0.01 M Tris-buffer, 0.15 M NaCl and 0.001 M disodium ethylenediamine tetraacetate (EDTA), pH 7.4]; the cells were filtered through 153 μm nylon filters. Cauda from mice 30 dpp or older were minced in 2 ml TNE and cauda from younger mice were minced in 0.5 ml TNE buffer to provide a reasonable cell concentration for FCM measurements.

For morphology studies, two independent 0.1 ml aliquots from each filtered cauda sperm sample were removed, placed in separate 12 × 75 mm plastic conical test tubes, stained with an equal volume of Eosin-Y (1% in water), smeared onto glass slides and air-dried. Slides were dipped into methanol to remove excess stain and mounted with coverslips using Permount (Fisher Scientific Co., Fair Lawn, NJ). When sperm were present in the cauda samples, 350 intact sperm nuclei per animal (1000 cells per age group) were assayed for sperm head abnormalities according to criteria of Wyrobek and Bruce (1975).

Vas Deferens Sperm Cells

The vas deferens from mice 28 dpp and older were placed into 2.0 ml TNE and sperm were extruded from the vas by pressing a blunt probe along the length of the tubule. "Cords" of sperm obtained from animals of the same age were picked up with a Pasteur pipette and pooled in a 12 × 75 mm plastic test tube. Two separate aliquots from each pooled sample were prepared for morphology studies as described above.

Two-Step Acridine Orange Method

Cell staining. Two-hundred μl of each cellular suspension of testicular, cauda and pooled vas deferens samples containing approximately 1×10^6 cells/ml were admixed with 400-μl of a solution containing 0.08 N HCl, 0.15 M NaCl and 0.1% Triton X-100 (Sigma Chemical Co., St. Louis, MO). Triton X produces holes in the cell membranes, which facilitates equilibrium dye-staining; the low pH dissociates histones from histone-containing testicular cells (Evenson et al., 1980b) and apparently partially denatures sperm DNA (Evenson et al., 1985). Thirty sec later, 1.2 ml of a solution containing 0.2 M Na_2HPO_4—0.1 M citric acid buffer (pH 6.0), 1 mM EDTA, 0.15 M NaCl and 6 μg/ml of the metachromatic fluorochrome AO (Polysciences, Warrington, PA) was added to the sample according to the procedure of Darzynkiewicz et al. (1976).

Ribonuclease (RNase) Digestion

Aliquots of sperm in TNE (0.1 ml) were combined with equal volumes of HBSS containing 0.1% Triton X-100 and incubated 20 min (22°C) without or with 1500 units/ml RNase A (Cooper Biomedical, Malvern, PA). After incubation, the cells were placed at 4°C to inhibit further enzyme digestion, stained by the two-step AO procedure and measured by FCM.

Flow Cytometry

Immediately after AO staining, approximately 200 cells/sec were passed through the quartz flow channel of a Cytofluorograf II interfaced to a 2150 Data Handler (Ortho Diagnostics, Inc., Westwood, MA) and a Tektronix 4612 hard copier (Tektronix, Inc., Beaverton, OR). Recorded measurements were begun three min after staining. Red fluorescence ($F_{>600}$) and GF (F_{530}) emitted from individual cells were separated optically and the digitized signal was recorded in list mode on the computer disk. Data were based on 5×10^3 cells/sample.

RESULTS

Testicular Development

Testicular cells obtained from adult mice were placed in suspension, stained with AO, and measured by FCM. Two distinct subpopulations were demonstrated within each of the 2n and 4n cell types that are distinguished by differential amounts of RF (Fig. 1a). The 1n populations seen in Figure 1a and in the computer-enhanced scatterplot of Figure 1b can be classified as round, elongating, and elongated spermatids based on previous sorting experiments (Evenson et al., 1985). Mean proportions ± 1 standard deviation (SD) of 1n (85.1 ± 1.6), 2n (7.3 ± .8), and 4n (7.7 ± 1.2); and round (40.4 ± 5.6), elongating (25.3 ± 4.4), and elongated (34.4 ± 2.3) spermatid populations used as control values were based on independent samples from 19 adult male mice. Light microscope evaluation of these samples revealed a negligible presence of Leydig and other interstitial cells. Also, no difference was observed in the percentage of 2n and 4n cells present between minced decapsulated and nondecapsulated testes. Collagenase was not used to liberate testis cells; therefore, it is assumed that 2n

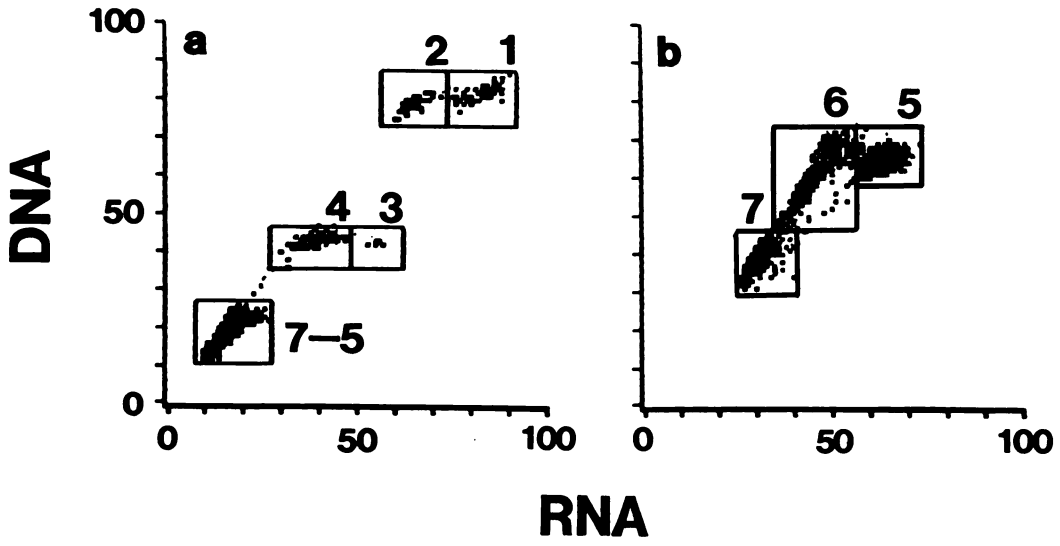

FIG. 1. Scatterplots of RF (*RNA*) vs. GF (*DNA*) integrated area signals of AO-stained testicular cells obtained from a 104-dpp mouse. (*a*) The overall distribution of 4n (*boxes 1* and *2*), 2n (*boxes 3* and *4*) and 1n (*boxes 5–7*) cells from minced testes. (*b*) Computer enhancement of 1n population showing the relation of round (*box 5*), elongating (*box 6*), and elongated spermatids (*box 7*).

and 4n populations contain primarily seminiferous epithelial cells which are more easily liberated by mechanical disruption than are somatic interstitial cells. Dual parameter measurements of AO-stained cells provide easy classification of testicular cells into seven or eight types.

Figure 2 displays representative histograms of GF frequency showing changes in proportion of 1n, 2n, and 4n cell populations in the developing testis of male mice. Testes from 2 to 10 dpp mice exhibited one major GF peak (90% cells, 2n, channel 40) and one minor peak (10% cells, 4n, channels 70–80). From 12 to 18 dpp, the ratio of 2n to 4n cells decreased; by 18 dpp, three definite populations (1n, 2n, and 4n cells) were observed. By 30 dpp, testicular samples exhibited two distinct peaks within the 1n population consisting of round and elongating spermatids at channel 20 and elongated spermatids at channel 14. After 30 dpp, the proportion of elongated spermatids continued to increase.

The ratio of the three testicular populations present for each time point is shown in Figure 3. Note that the initial appearance of 1n cells at 18 dpp was coincident with the maximal number of the 4n cells. The 1n population increased steadily through 48 dpp and reached an 85% plateau level.

A time-dependent change in distribution of the 4n population is illustrated in Figure 4, which displays scatterplots of RF area vs. GF area for testicular cells sampled from 2, 4, 8, 18, and 22 dpp and control animals. The 4n cells from 2 dpp consisted of a relatively homogeneous cell cluster in box 2 comprising 8–9% of total cells. At 4 and 8 dpp, two distinct 4n populations (boxes 1 and 2) differing in RF were evident. The ratio of cells in box 2 to those in box 1 at 4 and 8 dpp was 4.7:1 and 1.5:1, respectively. When 1n cells were first detected at 18 dpp, 4n cells represented 43% of the entire testicular population, and the ratio of cells in box 2 to those in box 1 was 2.3:1. At 22 dpp, when the 4n population was at a maximum 58%, this ratio was 1.9:1. For control adult animals, this ratio was 0.8:1, with 4n cells comprising 8% of the testicular population.

Developmental changes in the three major spermatid populations from 18 through 100 dpp are shown in Figure 5. The 1n cells present between 18 and 24 dpp have staining characteristics consistent with round spermatids. Note the *relative* percentage of decrease in this population as the elongating population appeared, and the drop in percentage of the elongating population as the elongated population appears.

S Phase Cells

Cells with GF values between those of the 2n and 4n populations (Figs. 2,4) were progressing through S phase of the cell cycle. From 4 to 8 dpp, RF signals from the S phase cells became more dispersed (Fig.

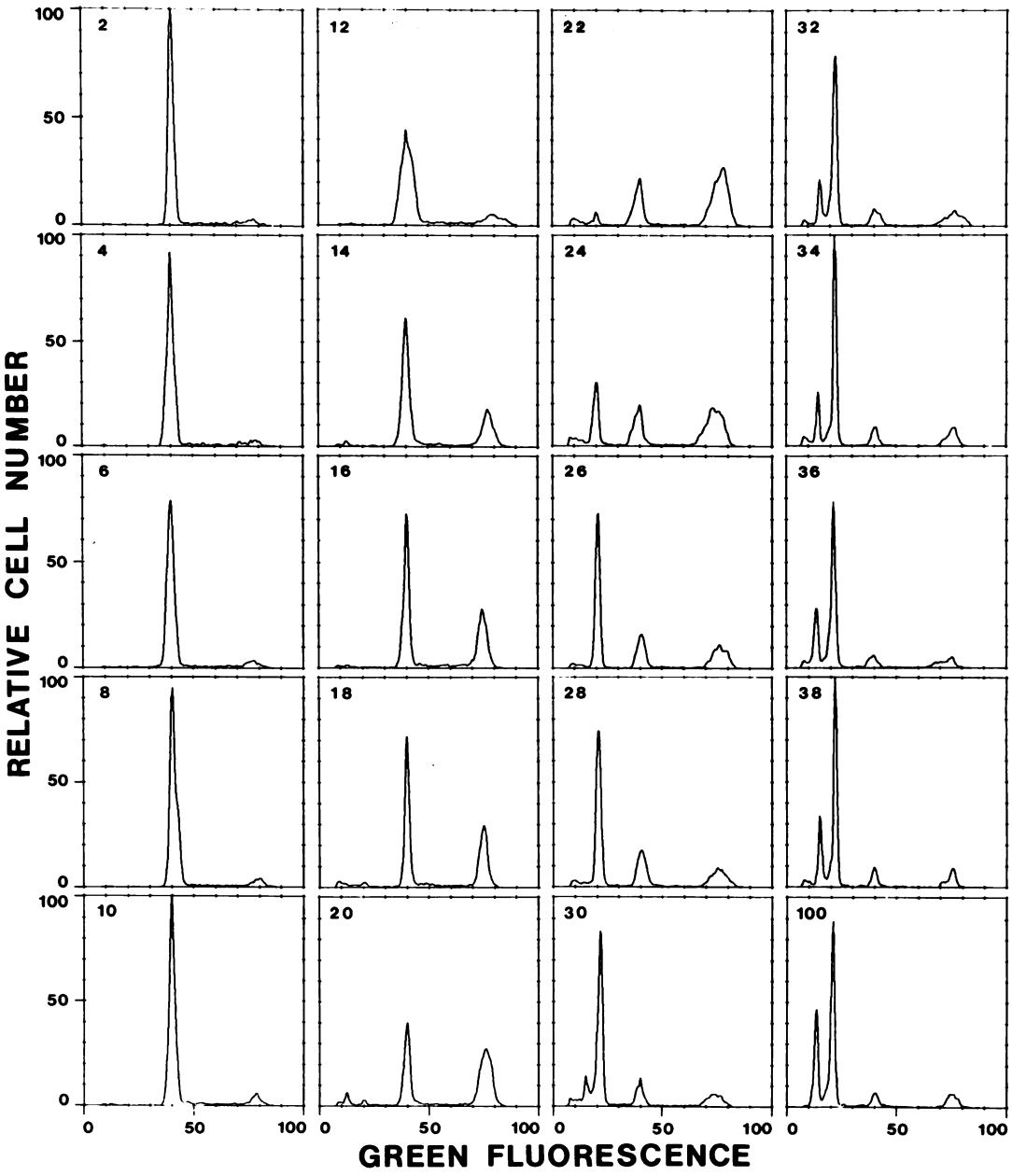

FIG. 2. Histograms of GF derived from AO-stained testicular cells (5000 cells/histogram) sampled between 2 and 100 dpp. The *numbers* in the *upper left corners* correspond to dpp age. *Peaks* at *GF channels* 14–20, 40, and 70–80 represent 1n, 2n, and 4n cells, respectively.

4), most likely due to DNA synthesis occurring in different cell types that contained varying amounts of RNA.

The proportion of S phase cells decreased between 2 and 10 dpp from 7% to 3% (Fig. 6). Between 10 and 12 dpp, this proportion increased rapidly to approximately 9%, where it remained through 18 dpp. After 18 dpp, the ratio of S phase cells decreased steadily until 30 dpp when adult levels were attained.

Cauda Sperm Cells

Initial appearance of 1n cells in the cauda was a relatively variable phenomenon. Although all samples obtained from 30- 32- and 34-dpp animals contained some cells which corresponded both in fluorescence (Fig. 7) and cytology to sperm, the numbers present were small; therefore, the mean values of the population had a high SD (Figs. 8,9). The 3 animals within each of these groups exhibited similar testicular

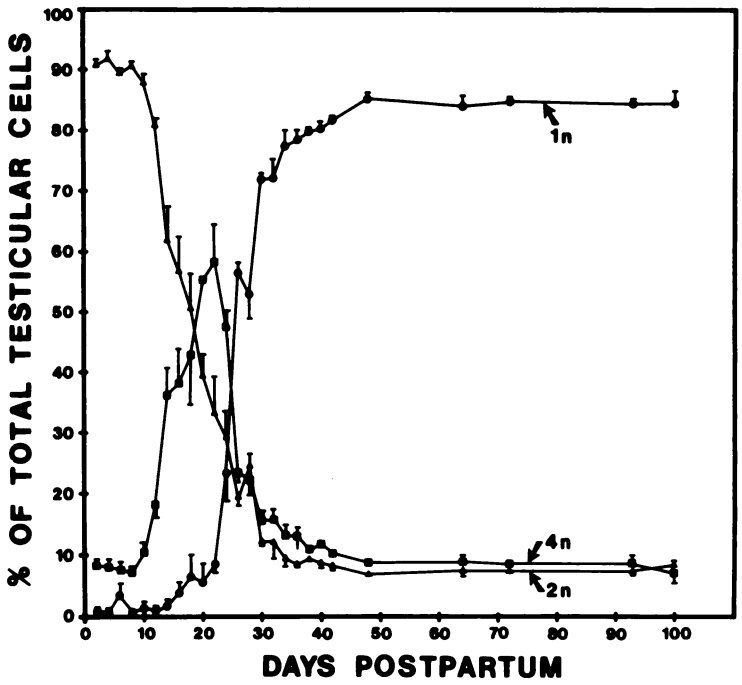

FIG. 3. Plots of mean values ± SD (n=3) for proportions of 1n, 2n and 4n *testicular cells* sampled between 2 and 100 *dpp*. Individual cells were classified on the basis of their RF and GF.

development, as indicated by small SD about the mean percentage for the three testicular cell populations measured (Fig. 3). By 36 dpp, all animals apparently contained a large number of 1n sperm in the cauda; however, only a portion of these (59 ± 22%) emitted fluorescent signals characteristic of normal adult spermatozoa populations (Fig. 7). By 38 dpp, most of the 1n cells (95 ± 1.3%) in the cauda produced fluorescent signals that fell within the normal spermatozoa range. In addition to mature sperm cells, the cauda of 30- to 36-dpp mice contained some round, elongating, and elongated spermatids, as determined by fluorescence values of AO-stained cells and light microscopy.

The mean percentages of cauda sperm exhibiting abnormal head morphology (Fig. 8) at 30, 32, 34, and 36 dpp were 34.1, 63.5, 89.2, and 90.2, respectively; however, because of low concentrations of sperm in the cauda samples at these ages, the total number of cells scored by completely scanning both slides from each animal at 30, 32, and 34 dpp was 214, 30, and 807, respectively. Due to the limited number of animals and cells examined, no solid conclusion can be drawn concerning the initial pattern of appearance for abnormal sperm head morphology. Frequency of cauda sperm exhibiting abnormal head morphology was 55% at 38 dpp, but rapidly decreased between 38 and 48 dpp to a value of 6.7%. By 64 dpp, frequency of occurrence of sperm head abnormalities decreased to 1.7%, which fell within the 1.2–3.4% observed for normal adult males of this strain (Wyrobek and Bruce, 1975). In addition, structures similar to detached flagella (Albert and Roussel, 1983) or threadlike spermatozoa (Krzanowska, 1981) were frequently observed.

Due to the metachromatic staining properties of AO, abnormal conformation of sperm cell chromatin can be determined (Evenson et al., 1980a). The ratio of RF to total fluorescence (RF + GF), termed α_t (Darzynkiewicz et al., 1975), provides an index for the susceptibility of DNA in situ to partial denaturation after low pH treatment of the two-step AO technique.

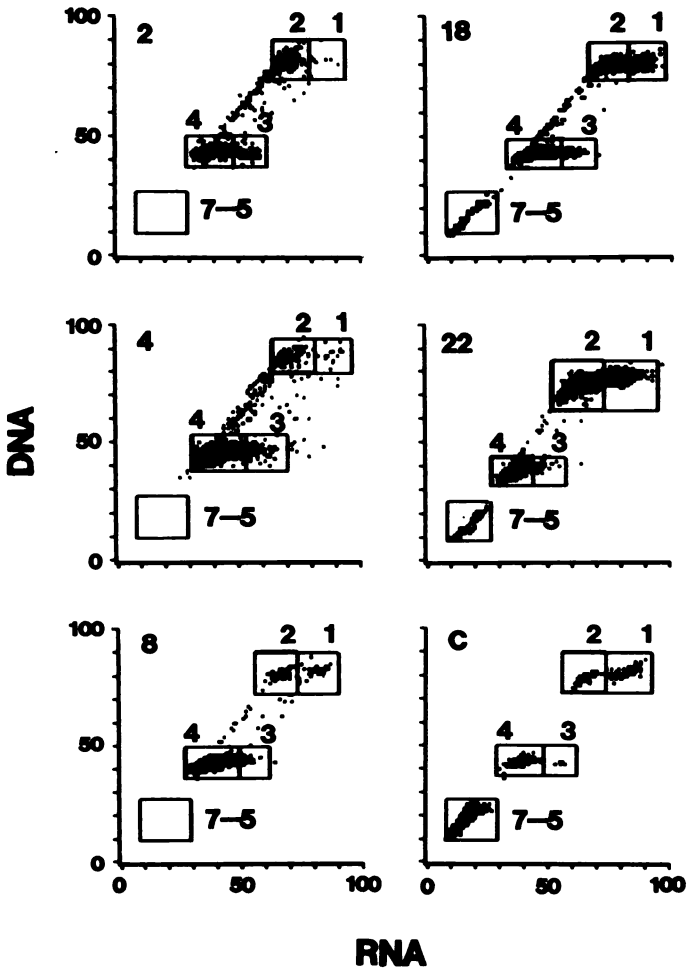

FIG. 4. Representative scatterplots of RF (*RNA*) vs. GF (*DNA*) integrated area signals for AO-stained testicular cells. Comparison of plots from 2 through 22 dpp (*numbers* in *upper left hand corners* correspond to dpp age) and adult control show the time-dependent changes of the RF component.

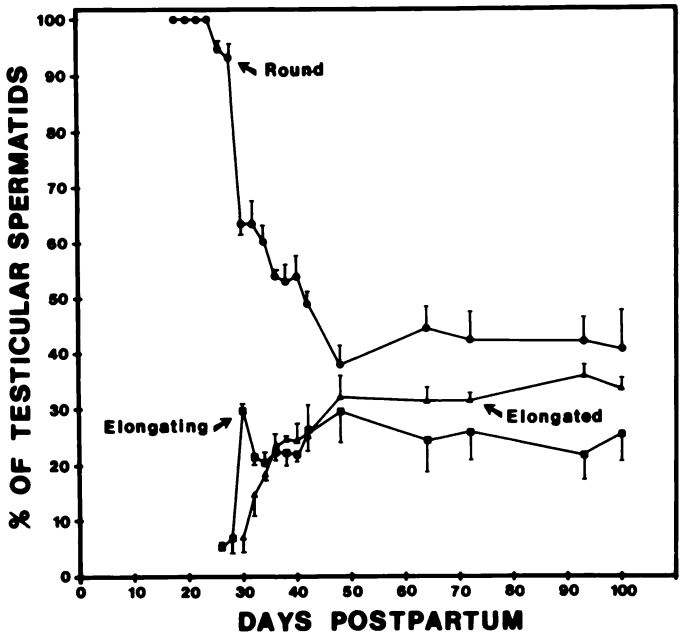

FIG. 5. Plots of the change in average values ± SD (n=3) for proportions of *round, elongating,* and *elongated spermatids* between 18 and 100 *dpp.* Individual cells were classified according to their RF vs. GF integrated area signals.

Confidence Intervals (CI) using average values ± 1 SD for mean ($\bar{X}$) of α_t, (0.24 ± 0.02), GF (434 ± 26) and RF (140 ± 15); SD of α_t (0.02 ± 0.01); and coefficient of variation (CV) of α_t (9.8 ± 2.5), used as control values, were computed from independent measurements of 9 adult animals killed over the course of this study. Time-dependent changes in these parameters derived from cauda sperm samples are shown in Figures 8 and 9. The $\bar{X}$, CV, and SD of α_t all decreased substantially from 30 through 100 dpp. These decreases were accompanied by a decrease in RF and a slight change in GF. Major decreases in $\bar{X}$ value of α_t and RF (Figs. 8,9) occurred between 34 and 38 dpp. After 38 dpp, these values remained within the control CI.

The $\bar{X}$ of GF, RF, and α_t, from 35-dpp cauda sperm compared to adult control values (35-dpp sample/adult control sample) were 1.19, 2.33 and 1.53, respectively. RNase digestion had no effect on these values, indicating that increased RF and α_t values were due to increased susceptibility of chromatin from 35-dpp cauda sperm to acid denaturation of DNA in situ and not to abnormal RNA retention.

Vas Deferens Sperm

Results of microscopic examination of samples taken 30–34 dpp agreed with FCM measurements indicating that these samples were azoospermic. Percentages of sperm head abnormalities among vas deferens sperm from 36 to 93 dpp are shown in Figure 10. At 36 dpp, 89% of vas deferens sperm exhibited abnormal head morphologies; however, this percentage dropped steadily to 2.4% by 64 dpp and then remained constant.

A distinct population of 1n cells was first detected by FCM in the pooled vas deferens sperm taken at 36 dpp. Fluorescent signals indicated that 98% of these cells were substantially lower in GF than normal sperm (Figs. 7, 11, 12). By 38 dpp, the 1n population of the vas deferens was divided into two distinct populations differing greatly in their fluorescence characteristics (Fig. 11). Eighty-nine percent of the cells (Fig. 11) had the lower GF observed at 36 dpp, while 11% produced fluorescent signals characteristic of normal sperm. Between 38 and 64 dpp, a progressive increase in proportion of 1n cells with higher GF occurred. Over 90% of the 1n cells produced a normal GF signal at ⩾64 dpp.

DISCUSSION

The three major phases of spermatogenesis can be distinguished clearly by comparing fluorescent properties of AO-stained testicular cell populations obtained from prepubertal male mice. Histograms of GF frequency shown in Figure 2 can be divided into three groups: 2 to 8 dpp, 8 to 18 dpp, and 18 to 30 dpp, corresponding to spermatogonial proliferation, meiosis, and spermiogenesis, respectively.

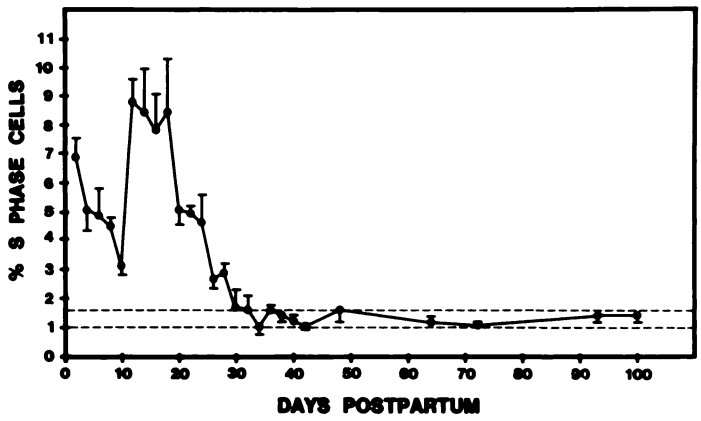

FIG. 6. Graphic representation of change in average percent ± SD for S *phase cells* from 2 through 100 dpp. The two *parallel dashed lines* indicate the upper (1.6%) and lower (1.0%) limit for a 99.9% CI established about mean value (1.3%) from 19 adult control animals.

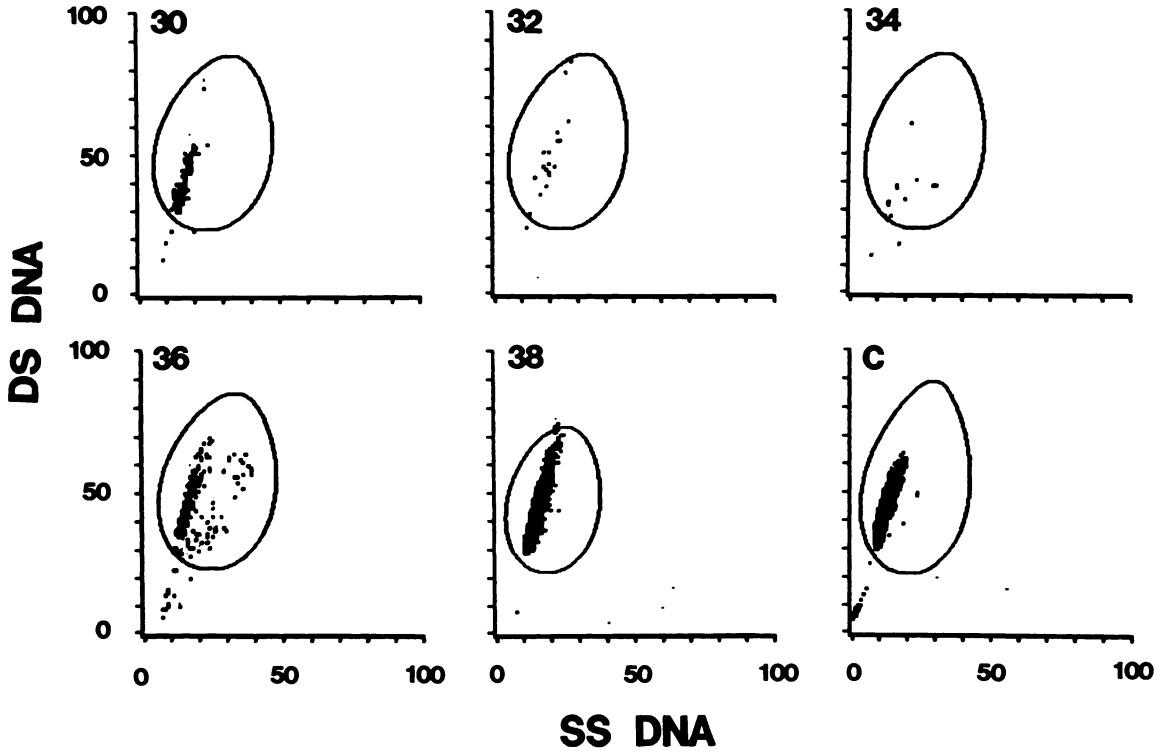

FIG. 7. Representative scatterplots of RF (*SS DNA*) area vs. GF (*DS DNA*) peak signals for AO-stained cauda samples, from early pubertal stages, 30–38 dpp (*numbers* in *upper left corners* correspond to dpp age and adult control (*c*). Each sample was minced, diluted in equal volumes of buffer, an approximate equal volume of stained sample was passed through the flow cytometer.

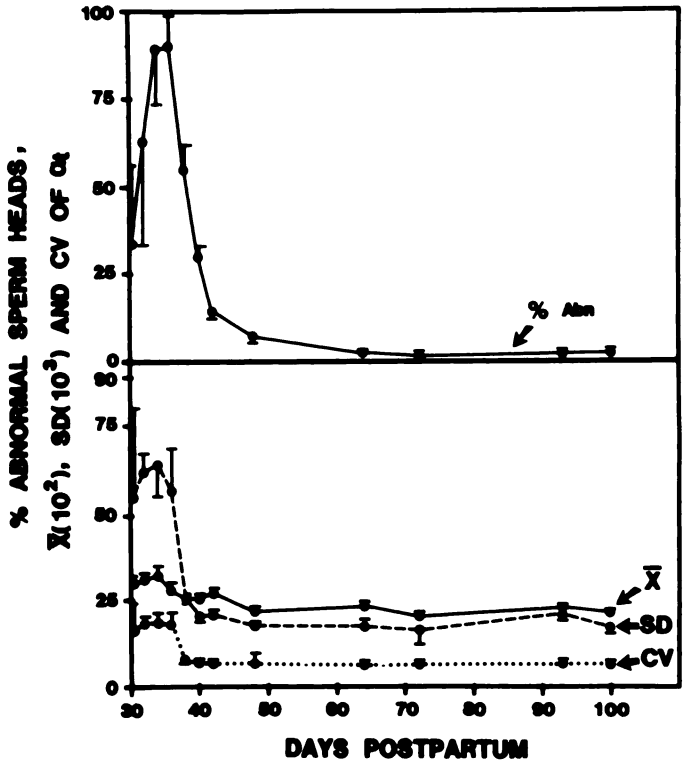

FIG. 8. Plots of time-dependent changes in percentage of cauda sperm with *abnormal head morphology*, $\bar{X}$ (10^2), SD (10^3), and CV of α_t for cauda sperm sampled from 30 to 100 dpp. Multipliers 10^2 and 10^3 for used with α_t and SD of α_t so they can be plotted on the same scale as CV of α_t. 99.9% CI for $\bar{X}$ (10^2), SD (10^3), and CV of α_t for control sperm are 21.4–27.3, 13.0–34.5, and 5.6–14.0, respectively (n=9).

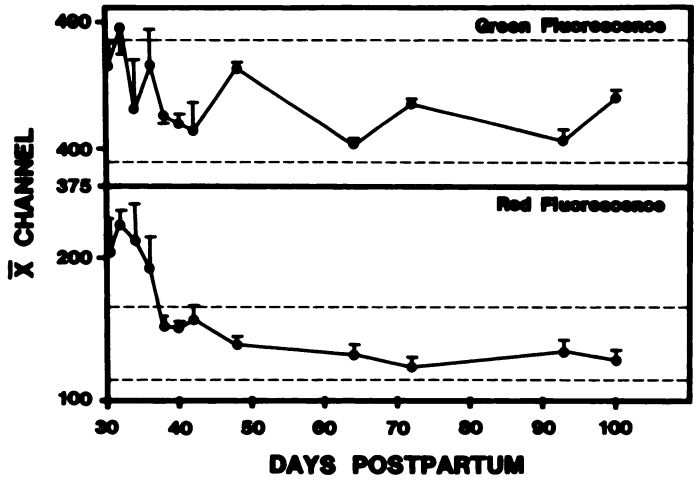

FIG. 9. Plots of RF and GF peak signals from AO-stained cauda sperm sampled on 30 through 100 dpp. *Horizontal parallel dashed lines* delimit 99.9% CI established about the mean values based on observations from 9 adult control animals.

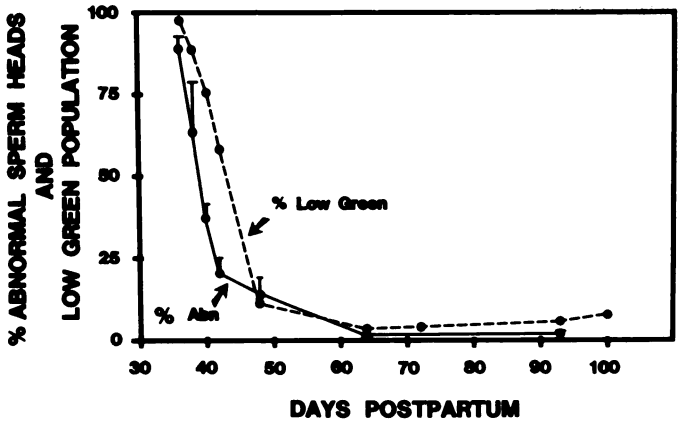

FIG. 10. Plots of time-dependent changes in *percentage of abnormal sperm heads* and percentage of AO-stained cells exhibiting *low GF* from vas deferens sperm sampled from 36 through 100 dpp.

Spermatogonial Proliferation

Dynamic changes in testicular populations during proliferation can be demonstrated by comparing RF vs. GF scatterplots of the 4n population shown in Figure 4 (boxes 1 and 2). By combining our observations with those made by other investigators, we can make certain predictions about the nature of these 4n cell types. At 2 dpp, the testis contains actively proliferating Sertoli cells (Clermont and Perey, 1957); the presence of a single 4n population (box 2) probably reflects the G_2/M phases of these supportive cells. By 4 dpp, gonocytes are proliferating and spermatogonial division attains adult levels of efficiency with development of primitive type A spermatogonia (Clermont and Perey, 1957; Nebel et al., 1961; Setchell, 1978). The appearance of cells in box 1, which have a higher RF than those in box 2, is concurrent with this initial increase in spermatogonial division, and probably reflects proliferation of the relatively large (14–16 μm; Bellvé et al., 1977), RNA-rich (Monesi, 1965; Fox and Fox, 1967), primitive type A spermatogonia. The increase in cells in box 1 from 4 through 8 dpp is concurrent with continuing spermatogonial proliferation when type A, intermediate, and type B spermatogonia appear (Clermont and Perey, 1957; Bellvé et al., 1977).

Meiosis

The increase in the 4n population first noted at 10 dpp (Figs. 2,5) is concurrent with the onset of meiosis (Bellvé et al., 1977). Since Sertoli cells stop proliferation at 12 dpp (Clermont and Perey, 1957; Bellvé et al., 1977; Kluin et al., 1984) and mitotic division of spermatogonia between 13 and 84 dpp occurs at a relatively slow rate (Kluin et al., 1984), this increase in 4n and accompanying decrease in 2n populations probably result from an accumulation of primary spermatocytes in progressive stages of meiotic prophase (Clermont and Perey, 1957; Bellvé et al., 1977).

After 12 dpp, cells shown in box 2 (Fig. 4) are attributed to spermatogonial differentiation resulting in progressively smaller cells (Bellvé et al., 1977) with successive reductions in RNA synthesis (Monesi, 1965; Fox and Fox, 1967). Cells progressing through pachytene of meiotic prophase I exhibit a 1.5-fold increase in size, producing cells larger than primitive type A spermatogonia (Bellvé et al., 1977), and a

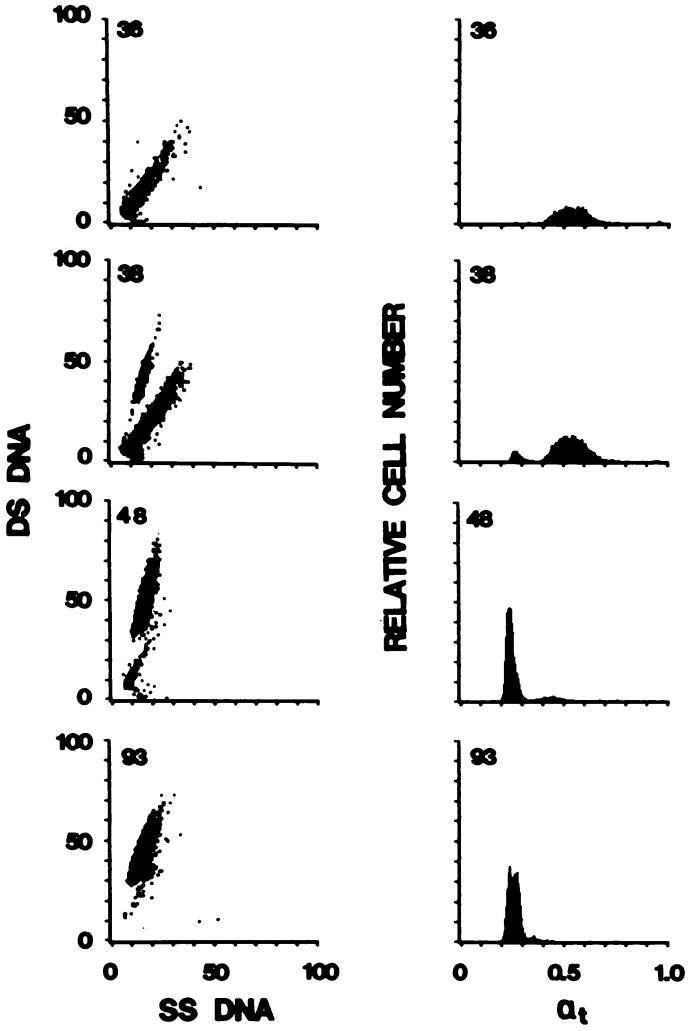

FIG. 11. Representative scatterplots of RF (*SS DNA*) vs. GF (*DS DNA*) peak signals and histograms of α_t for vas deferens sperm stained with AO and sampled at 36, 38, 48 and 93 dpp.

concurrent step-wise increase in RNA synthesis becoming maximal at midpachytene (Monesi, 1965). These cells should have increasing levels of RNA; by late pachytene, they would be expected to produce the higher RF signals characteristic of cells in box 1.

The appearance of round spermatids on 18 dpp marks completion of the first meiosis. The short duration of the first meiosis (8 days) in the testes of young animals compared to adult testes (14 days; Oakberg, 1956b; Fox and Fox, 1967) is consistent with data from Bellvé et al., (1977) and may result from a temporal reduction in type B spermatogonia and preleptotene stages (Nebel et al., 1961).

Spermiogenesis

The appearance of round spermatids at 18 dpp (Figs. 2,5) also marked the beginning of the first round of spermiogenesis, which continued through 28–30 dpp, and was completed by 30 dpp when elongated spermatids were first detected. During this period significant changes in the 1n, 2n and 4n testicular populations continued until 30 dpp when cell proportions approached adult levels. Time intervals (Fig. 5) for development of elongating spermatids from round spermatids (6–8 days), and elongated spermatids from elongating spermatids (2–4 days) during the first round of spermiogenesis in young animals are consistent with the schedule proposed by Oakberg (1956a,b) for adult mice.

Measurements by flow cytometry of testicular populations from mouse and rat (Clausen et al., 1977) demonstrate the following: 1) The proportion of 4n cells prior to completion of meiosis is much higher in mouse (37–40% at 15 dpp) than in rat (6% at 15 dpp). The 4n proportion supersedes the 2n frequency from 20 through 28 dpp in mouse, but is never greater in the rat. 2) The increase in 4n cell frequency, occurring during the first meiosis, becomes maximal three days sooner and is approximately 2-fold greater in mouse than in rat. 3) Spermatids are detected at least two days earlier in mouse (18 dpp). Spermatid frequency in both species remains constant 3–4 days following their initial appearance, and then steadily increases to adult levels. 4) Frequencies of 1n, 2n and 4n cell populations reach adult levels by 48 dpp in mouse. These frequencies approach adult levels by 40 dpp in rat. 5) Adult frequencies for 1n, 2n and 4n cells are similar for both species, although frequency of 2n cells appears to be slightly larger in rat.

Epididymal Sperm

A comparison of the distribution pattern of fluorescence of AO-stained epididymal cells obtained from adult and 30-dpp mice (Fig. 7) demonstrates the presence of epididymal sperm by 30 dpp, which is 4–6 days earlier than seen by Albert and Roussel (1983). Although this difference could be due partly to strain differences, it is more likely a result of greater sensitivity of FCM over light microscopy for detection of near azoospermic samples (Evenson and Melamed, 1983).

The first cauda spermatozoa appeared at 30 dpp; this is earlier than would be predicted based on the 34.5-day duration of spermatogenesis estimated for adult mice (Oakberg, 1956a,b; Fox and Fox, 1967), and the 28–30-day period required for cells labeled with [^{3}H]-thymidine at the preleptotene stage to undergo meiosis and spermiogenesis and arrive in the cauda of adult mice (Sega, 1974). Observations reported here and those of Bellvé et al., (1977) strongly suggest that the first round of meiosis in young mice is no longer than 8 days, i.e., approximately 6 days shorter than the estimates for adult animals (Oakberg, 1956a,b; Fox and Fox, 1967). Since our observations indicate that the first round of spermiogenesis occurs at about the same rate as in adult mice, the apparent early arrival of sperm from the first round of spermatogenesis into the cauda is most likely attributable to an accelerated rate of meiosis in young testicular tissue compared to that in adult testicular tissue. Sperm from any one round of spermatogenesis in the adult must contend with products of previous rounds while the sperm travel through the epididymis. Between 28 and 30 dpp, the first wave of sperm is moving into the epididymis; with unimpeded movement they may traverse the caput and corpus at a faster rate than the 3 days (Sega, 1974) observed in the adult. The high incidence of abnormalities in cauda sperm head morphology and the appearance of large numbers of detached flagella (or threadlike spermatozoa) in B6C3F$_1$/J pubertal mice are also characteristic of the initiation of sperm production in other strains (Krzanowska, 1981; Albert and Roussel, 1983).

The time-dependent reduction in α_t and RF values (Figs. 8,9) indicates that differences in nuclear chromatin structure exists between caudal sperm cell populations measured at the beginning of puberty (30–36 dpp) and those measured during later stages of maturational development (48–100 dpp).

Changes in percentage of abnormal head morphologies between 30 and 36 dpp (Fig. 8) parallel changes in RF and α_t showing a high correlation between chromatin structure and sperm head morphology. Previous studies have shown a high correlation between toxic chemical-induced abnormalities of sperm head morphology and chromatin structure (Evenson et al., 1985, 1986a).

Vas Deferens Sperm

The 1n populations from pooled vas deferens samples between 36 and about 64 dpp contain two distinct subpopulations (Fig. 11) differing in their relative GF, RF, and α_t values. The population with the initially, abnormally low GF dramatically decreases in frequency between 36 and 64 dpp and then remains constant below 10%. This change is concurrent with time-dependent increases in the percentage of sperm exhibiting normal head morphology reported here (Fig. 11) and elsewhere (Krzanowska, 1981; Albert and Roussel, 1983), and is consistent with the interpretation that cells which produce the higher GF are normal sperm. Red fluorescence remained normal for this population from 36 to 100 dpp, indicating no abnormal susceptibility to acid denaturation in the DNA, and no abnormal retention of RNA.

Using dual parameter FCM measurements of AO-stained testicular, epididymal and vas deferens sperm cells, this study has characterized the kinetics of cellular changes in growing mice. This work provides an important basis for current studies evaluating the effects of exposure to chemical agents during different stages of reproductive development.

ACKNOWLEDGMENTS

The authors thank Rebecca K. Baer, Brenda E. Ballachey, and Russell W. Gesch for technical assistance and Elsa Wood for help preparing this manuscript.

REFERENCES

Albert M, Roussel C, 1983. Changes from puberty to adulthood in the concentration, motility, and morphology of mouse epididymal spermatozoa. Int J of Androl 6:446–60

Bellvé AR, Cavicchia JC, Millette CF, O'Brien DA, Bhatnagar YM, Dym M, 1977. Spermatogenic cells of the prepuberal mouse; isolation and morphological characterization. J Cell Biol 74:68–85

Balhorn R, Weston S, Thomas C, Wyrobek AJ, 1984. DNA packaging in mouse spermatids: synthesis of protamine variants and four transition proteins. Exp Cell Res 150:298–308

Carter SD, Hein JF, Rehnberg GL, Laskey JW, 1984. Effect of benomyl on the reproductive development of male rats. J of Toxicol Environ Health 13:53–68

Carter SD, Laskey JW, 1982. Effect of benomyl on reproduction in the male rat. Toxicol Lett 11:87–94

Cattanach BM, Pollard CE, Isaacson JH, 1968. Ethyl methane-sulfonate induced chromosome breaks in the mouse. Mutat Res 6:297–307

Clausen OPF, Purvis K, Hansson V, 1977. Application of microflow fluorometry to studies of meiosis in the male rat. Biol Reprod 17:555–60

Clermont Y, Perey B, 1957. Quantitative study of the cell population of the seminiferous tubules in immature rats. Am J Anat 100: 241–68

Darzynkiewicz Z, Evenson D, Kapuscinski J, Melamed MR, 1983. Denaturation of RNA and DNA *in situ* induced by acridine orange. Exp Cell Res 148:31–46

Darzynkiewicz Z, Traganos F, Sharpless T, Melamed MR, 1975. Thermal denaturation of DNA *in situ* as studied by acridine orange staining and automated cytofluorometry. Exp Cell Res 90:411–28

Darzynkiewicz Z, Traganos F, Sharpless T, Melamed MR, 1976. Lymphocyte stimulation: a rapid multiparameter analysis. Proc Natl Acad Sci USA 73:2881–84

Ehling UH, Cummings RB, Malling HV, 1968. Induction of dominant lethal mutations by alkylating agents in male mice. Mutat Res 5:417–28

Evenson DP, Baer RK, Jost LK, Gesch RW, 1986a. Toxicity of thiotepa on mouse spermatogenesis as determined by dual parameter flow cytometry. Toxicol Appl Pharmacol 82:151–63

Evenson DP, Darzynkiewicz Z, Jost L, Janca F, Ballachey B, 1986b. Changes in accessibility of DNA *in situ* to various fluorochromes during spermatogenesis. Cytometry 7:45–53

Evenson DP, Darzynkiewicz Z, Melamed MR, 1980a. Relation of mammalian sperm chromatin heterogeneity to fertility. Science 240:1131–33

Evenson DP, Darzynkiewicz Z, Melamed MR, 1980b. Comparison of human and mouse sperm chromatin structure by flow cytometry. Chromosoma 78:225–38

Evenson DP, Higgins PH, Grueneberg D, Ballachey B, 1985. Flow cytometric analysis of mouse spermatogenic function following exposure to ethylnitrosourea. Cytometry 6:238–53

Evenson DP, Melamed MR, 1983. Rapid analysis of normal and abnormal cell types in human semen and testis biopsies by flow cytometry. J Histochem Cytochem 31:248–53

Fox BW, Fox M, 1967. Biochemical aspects of the actions of drugs on spermatogenesis. In: Acheson GH (ed.), Pharmacological Reviews, Vol. 19. Baltimore: The Williams and Wilkins Co., pp. 21–57

Gledhill BL, Lake S, Dean PN, 1979. Flow cytometry and sorting of sperm and other male germ cells. In: Melamed MR, Mullaney PF, Mendelsohn ML (eds.), Flow Cytometry and Sorting. New York: John Wiley and Sons, pp. 471–84

Kleene KC, Distel RJ, Hecht NB, 1984. Translational regulation and adenylation of a protamine mRNA during spermiogenesis in the mouse. Dev Biol 105:71–79

Kluin PhM, Kramer MF, de Rooij DG, 1984. Proliferation of spermatogonia and Sertoli cells in maturing mice. Anat Embryol 169:73–78

Krzanowska H, 1981. Sperm head abnormalities in relation to the age and strain of mice. J Reprod Fert 62:385–92

Millette CF, Bellvé AR, 1977. Temporal expression of membrane antigens during mouse spermatogenesis. J Cell Biol 74:86–97

Monesi V, 1965. Synthetic activities during spermatogenesis in the mouse: RNA and protein. Exp Cell Res 39:197–224

Nebel BR, Amarose AP, Hackett EM, 1961. Calendar of gametogenic development in the prepuberal male mouse. Science 134:832–33

Oakberg EF, 1956a. A description of spermiogenesis in the mouse and its use in analysis of the cycle of the seminiferous epithelium and germ cell renewal. Am J Anat 99:391–413

Oakberg EF, 1956b. Duration of spermatogenesis in the mouse and timing of stages of the cycle of the seminiferous epithelium. Am J Anat 99:507–16

Roosen-Runge EC, 1977. The Process of Spermatogenesis in Animals. New York: Cambridge University Press

Schierbeek A, 1959. Measuring the Invisible World. New York: Abelard-Schuman, Ltd.

Sega GA, 1974. Unscheduled DNA synthesis in the germ cells of male mice exposed *in vivo* to the chemical mutagen ethyl methanesulfonate. Proc Nat Acad Sci USA 71:4955–59

Setchell BP, 1978. Spermatogenesis. *In* "The Mammalian Testis." Ithaca: Cornell University Press, pp. 181–232

Wyrobek AJ, Bruce WR, 1975. Chemical induction of sperm abnormalities in mice. Proc Natl Acad Sci USA 72:4425–29